AIP | The Journal of Chemical Physics

A photoelectron spectroscopy and density functional study of di-tantalum boride clusters: $Ta_2B_x^-$ (x = 2–5)

Lu Xie, Wei-Li Li, Constantin Romanescu, Xin Huang, and Lai-Sheng Wang

Citation: J. Chem. Phys. **138**, 034308 (2013); doi: 10.1063/1.4776769
View online: http://dx.doi.org/10.1063/1.4776769
View Table of Contents: http://jcp.aip.org/resource/1/JCPSA6/v138/i3
Published by the American Institute of Physics.

A photoelectron spectroscopy and density functional study of di-tantalum boride clusters: $Ta_2B_x^-$ ($x = 2$–5)

Lu Xie,[1] Wei-Li Li,[2] Constantin Romanescu,[2] Xin Huang,[1,3,a)] and Lai-Sheng Wang[2,b)]
[1]*Department of Chemistry, Fuzhou University, Fuzhou, Fujian 350108, People's Republic of China*
[2]*Department of Chemistry, Brown University, Providence, Rhode Island 02912, USA*
[3]*Fujian Provincial Key Laboratory of Theoretical and Computational Chemistry, Xiamen, Fujian 361005, People's Republic of China*

(Received 12 November 2012; accepted 4 January 2013; published online 17 January 2013)

The structural and electronic properties for di-tantalum boride clusters $Ta_2B_x^-$ ($x = 2$–5) were investigated using photoelectron spectroscopy and density functional calculations. The photoelectron spectra for $Ta_2B_x^-$ ($x = 2$–5) are obtained at several photon energies with rich spectral features. Density functional theory calculations are performed at the BP86 level to search for the global minima of both the anionic and neutral clusters. The calculated vertical electron detachment energies for the global minimum and low-lying isomers are compared with the experimental data. Strong boron-boron bonding is found to dominate the lowest energy structures of $Ta_2B_x^-$ and Ta_2B_x ($x = 2$–5), which are shown to be bipyramidal with the boron atoms forming an equatorial belt around the Ta–Ta dimer. Strong Ta–Ta bonding is observed in $Ta_2B_x^-$ and Ta_2B_x for $x = 2$–4, whereas the Ta–Ta distance is increased significantly in $Ta_2B_5^-$ and Ta_2B_5. © *2013 American Institute of Physics*. [http://dx.doi.org/10.1063/1.4776769]

I. INTRODUCTION

Bulk boron and metal borides have wide applications as refractory materials, ceramics, and superhard materials and have attracted sustained research interests over the past decades.[1–4] Because of its electron deficiency, bulk boron, boron compounds, and boron clusters all possess unusual chemical bonding and physicochemical properties. In particular, photoelectron spectroscopy (PES) in conjunction with theoretical calculations has revealed in recent years that boron clusters are planar up to at least B_{23}^-,[5–11] whereas for B_n^+ clusters the planar structures are found up to $n = 16$,[12] in contrast to bulk boron or boranes where three-dimensional (3D) cage-like structures are prevalent. Among the planar boron clusters, B_8^{2-} (D_{7h}) and B_9^- (D_{8h}) are found to be perfect molecular wheels, each with 6σ and 6π delocalized electrons, rendering them doubly aromatic.[5] Replacing the central boron atom by a carbon atom led to local minima for D_{6h} CB_6^{2-} and D_{7h} CB_7^-.[13,14] Valance isoelectronic substitution by an Al atom shows that Al avoids the central position in all AlB_n^- ($n = 6$–11) clusters.[15–17] However, transition metal atoms have been found experimentally and computationally to form metal-centered boron wheels ($M©B_n^-$)[18–20] and an electronic design principle has been advanced, according to the double aromaticity requirements, to construct and rationalize the electronic stability of these unique borometallic wheel-type complexes. Transition metal doped boron rings had been studied computationally by a number of authors.[21–25] The first metal-centered molecular wheels observed experimentally are $Co©B_8^-$ and $Ru©B_9^-$,[18] followed by the finding of two neutral clusters, Rh©B_9 and Ir©B_9,[19] according to the electronic design principle. The largest boron ring to form the molecular wheels is discovered to be B_{10} in $Ta©B_{10}^-$ and $Nb©B_{10}^-$,[20] which are also doubly aromatic with 10 σ and 6 π delocalized electrons. On the other hand, the isoelectronic 3d vanadium atom is found to be too small to stabilize a B_{10} ring.[26] Recently, a planar B_6 ring is found to be the building blocks in a complex metal boride crystal, $Ti_7Rh_4Ir_2B_8$,[27] suggesting some of the novel gaseous boron and boride clusters may be synthesized in the bulk.

Despite the recent advances of transition metal doped boron clusters, relatively little is known about the di-metal doped boron clusters. A theoretical investigation on the triatomic Li_2B species was reported previously.[28] The di-auride $Au_2B_7^-$ cluster has been studied[29] and found to possess a stable planar structure, similar to $H_2B_7^-$.[30,31] In the current work, we investigate the structural and electronic properties for the di-tantalum doped boron clusters $Ta_2B_x^-$ ($x = 2$–5). Photoelectron spectra for these four clusters have been obtained at several detachment laser energies. Density functional theory (DFT) calculations at the BP86 level are performed to search for the global minima for $Ta_2B_x^-$ ($x = 2$–5) and their neutral counterparts. Theoretical results are compared with the experimental data to confirm the identified global minima and low-lying isomers. The boron atoms are found to form an equatorial fan around the Ta–Ta axis, giving rise to quasi-bipyramidal geometries for the lowest-energy structures of these di-tantalum boron clusters. Strong Ta–Ta bonding is observed for species with $x = 2$–4, whereas for $x = 5$ a significant increase of the Ta–Ta distance is observed. The current study provides important information about the competition among metal–metal, B–B, and metal–B bonding in boride clusters and sets the stage for further studies of more complex $M_xB_y^-$ type metal boride clusters.

a)Electronic mail: xhuang@fzu.edu.cn.
b)Electronic mail: lai-sheng_wang@brown.edu.

II. EXPERIMENTAL METHOD

The experiment was performed using a magnetic-bottle PES apparatus equipped with a laser vaporization cluster source, details of which have been published in Ref. 32. Briefly, $Ta_2B_x^-$ clusters were produced by laser vaporization of a disk target made of isotopically enriched ^{11}B (96%) and Ta powders. The clusters were entrained by the helium carrier gas and underwent a supersonic expansion to form a collimated cluster beam after passing through a 6 mm diameter skimmer. The cluster distribution and cooling were controlled by the time delay between the pulsed valves and the vaporization laser and the resident time of the clusters in the nozzle.[33] To achieve better cooling, some experiments were carried out using a mixture of 5% Ar in He as the carrier gas. This approach has been shown recently to produce cold Au cluster anions.[34] Negatively charged clusters were extracted from the cluster beam and analyzed with a time-of-flight mass spectrometer. The clusters of interest ($Ta_2B_x^-$, $x = 2$–5) were mass selected and decelerated before being intercepted by a photodetachment laser beam: 193 nm (6.424 eV) from an ArF excimer laser; and 266 nm (4.661 eV), 355 nm (3.496 eV), or 532 nm (2.331 eV) from a Nd:YAG laser. Photoelectrons were collected at nearly 100% efficiency by a magnetic bottle and analyzed in a 3.5 m long electron flight tube. The photoelectron spectra were calibrated using the atomic spectra of Au^-, Bi^-, and Pb^-. The electron kinetic energy resolution of the PES apparatus, $\Delta E_k/E_k$, is typically ~2.5%, that is ~25 meV for 1 eV electrons.

III. THEORETICAL METHODS

The DFT calculations were carried out at the BP86 level.[35,36] Global minima searches were performed using analytical gradients with the Stuttgart relativistic small core basis set and an effective core potential[37,38] augmented with two *f*-type and one *g*-type polarization functions for Ta [$\zeta(f) = 0.210$, 0.697; $\zeta(g) = 0.472$] as recommended by Martin and Sundermann[39] and the aug-cc-pVTZ basis set for boron.[40,41] The scalar relativistic effects, namely, the mass velocity and Darwin effects, were taken into account via the quasi-relativistic pseudopotentials. Vibrational frequency calculations were done to verify the nature of the stationary points. The low-lying isomers revealed by the searches were further evaluated via single point calculations at the coupled cluster CCSD(T) level[42–46] with the Ta/Stuttgart + 2*f*1*g*/B/aug-cc-pVTZ basis sets at the BP86 geometries. For open-shell systems, the R/UCCSD(T) approach was used, where a restricted open-shell Hartree-Fock (ROHF) calculation was initially performed and the spin constraint was relaxed in the correlation treatment. In addition, more accurate optimizations in CCSD(T) were carried out for some close-lying structures with the Ta/Stuttgart + 2*f*1*g*/B/aug-cc-pVTZ basis sets. All DFT calculations were done with the GAUSSIAN 03 software package,[47] and the coupled-cluster calculations were performed using the MOLPRO 2010.1 package.[48] Three-dimensional contours of the molecular orbitals (MOs) were visualized using the VMD software.[49] Different exchange-correlation functionals were tested for accuracy and consistency. The BP86 functional showed superior results in terms of electron binding energies and structures for $Ta_2B_x^-$ and Ta_2B_x ($x = 2$–5). Therefore, we used the results with the BP86 functional for our direct comparison with the experiment.

Vertical detachment energies (VDEs) were calculated using the generalized Koopmans' theorem by adding a correction term to the eigenvalues of the anion.[50] The correction term was calculated as $\delta E = E_1 - E_2 - \varepsilon_{HOMO}$, where E_1 and E_2 are the total energies of the anion and neutral, respectively, in their ground states at the anion equilibrium geometry, and ε_{HOMO} corresponds to the eigenvalue of the highest occupied molecular orbital (HOMO) of the anion.

IV. EXPERIMENTAL RESULTS

The photoelectron spectra of $Ta_2B_x^-$ ($x = 2$–5) are shown in Figs. 1–4, respectively, at three detachment energies (355, 266, and 193 nm). We also performed experiment at 532 nm. But the 532 nm spectra did not reveal additional electronic or vibrational features and are not shown. The detachment transitions are labeled with letters (X, A, B, ...) and the measured VDEs are given in Table I. In each spectrum, the band X represents the transition from the ground electronic state of the anion to that of the corresponding neutral species, and the higher binding energy bands (A, B, ...) denote transitions to excited electronic states of the neutral cluster.

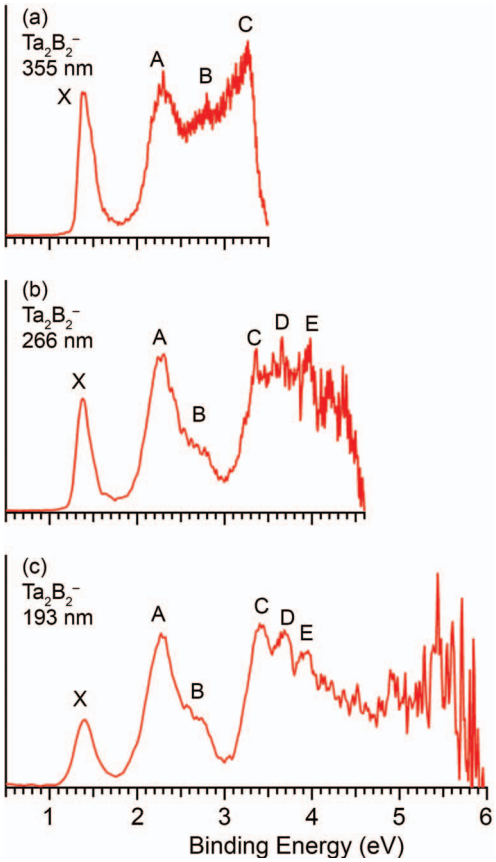

FIG. 1. Photoelectron spectra of $Ta_2B_2^-$ at (a) 355 nm, (b) 266 nm, and (c) 193 nm.

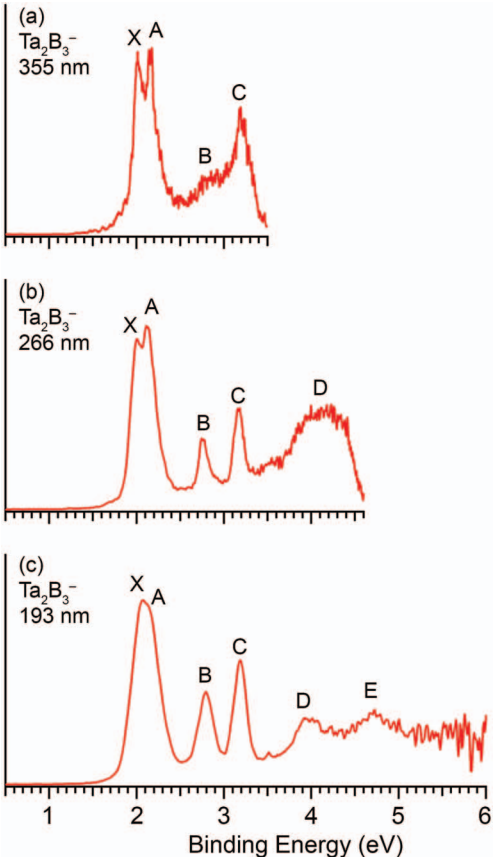

FIG. 2. Photoelectron spectra of $Ta_2B_3^-$ at (a) 355 nm, (b) 266 nm, and (c) 193 nm.

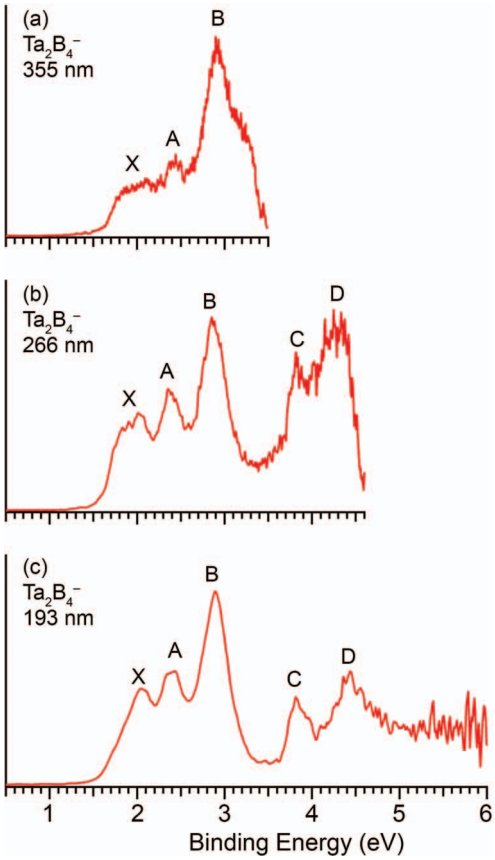

FIG. 3. Photoelectron spectra of $Ta_2B_4^-$ at (a) 355 nm, (b) 266 nm, and (c) 193 nm.

A. $Ta_2B_2^-$

The 355 nm spectrum of $Ta_2B_2^-$ (Fig. 1(a)) shows four detachment bands. Band X is relatively sharp with a VDE of 1.39 eV. Even at 532 nm, no vibrational fine features were resolved for band X, suggesting a possible low frequency vibrational progression. Because no vibrational features were resolved, the adiabatic detachment energy (ADE) was measured from the onset of the X band by drawing a straight line along the leading edge and then adding the spectral resolution to the intersection with the binding energy axis. The ADE obtained is 1.31 ± 0.04 eV, which also represents the electron affinity (EA) of neutral Ta_2B_2. Following a relatively large energy gap, three broad and congested bands (A, B, C) are observed. Band A has a VDE of 2.28 eV and its relative intensity increases with photon energies. The large X-A gap suggests that neutral Ta_2B_2 is likely a closed shell species with a HOMO-LUMO gap represented by the X-A gap. Band B (VDE: 2.78 eV) is relatively weak and is better resolved in the 266 and 193 nm spectra. The congested tail (labeled Band C) near the threshold of the 355 nm spectrum is likely due to thermionic emission,[51] as can be seen clearly in the 266 and 193 nm spectra, which show an energy gap after band B. The spectral features in the higher binding energy side are quite congested and three bands are tentatively labeled: C (VDE: 3.35 eV), D(VDE: 3.66 eV) and E(VDE: 3.98 eV).

B. $Ta_2B_3^-$

The 355 nm spectrum of $Ta_2B_3^-$ (Fig. 2(a)) reveals two well resolved bands, X and A, with VDEs of 2.00 eV and 2.16 eV, respectively. The ADE of the X band is measured to be 1.93 ± 0.03 eV, which also represents the EA of neutral Ta_2B_3. These two bands are relatively sharp, indicating a small geometry change between the ground state of $Ta_2B_3^-$ and the ground and first excited state of Ta_2B_3. Two more relatively weak and broad bands, B (VDE: 2.75 eV) and C (VDE: 3.17 eV), are observed in the 355 nm, but they are better defined in the 266 and 193 nm spectra. At the higher binding energy side, more congested spectral features are observed at 266 and 193 nm. Two bands, D (VDE: 3.96 eV) and E (VDE: 4.69 eV), are labeled. A relatively weak feature at ~3.5 eV is observed in the 193 nm spectrum (Fig. 2(c)), but are not labeled.

C. $Ta_2B_4^-$

The 355 nm spectrum of $Ta_2B_4^-$ (Fig. 3(a)) shows three broad bands: X (VDE: ~1.9 eV), A (VDE: 2.43 eV), and B (VDE: 2.88 eV). The ADE of the X band is estimated to be 1.70 ± 0.07 eV, which represents the EA of Ta_2B_4. The broad widths of these three bands indicate that there are multiple transitions in each band and/or a very large geometry change upon detachment. Following a large energy gap, the 266 and 193 nm spectra reveal a band C (VDE: 3.81 eV) and a broad

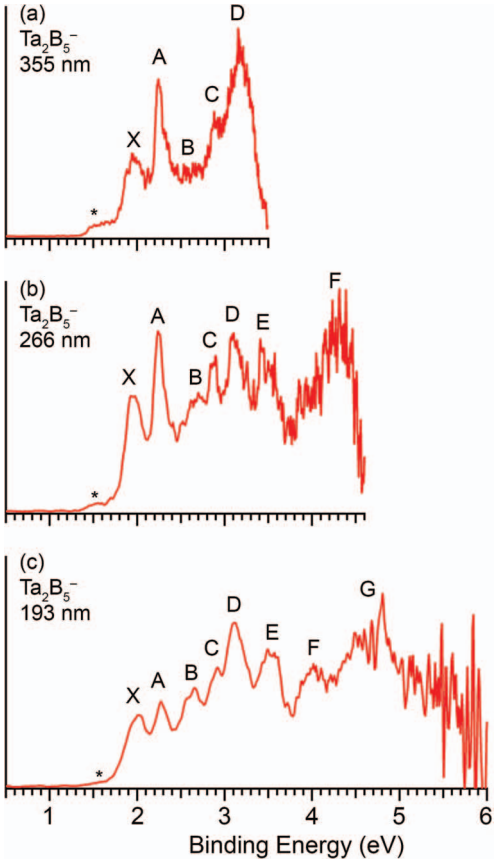

FIG. 4. Photoelectron spectra of $Ta_2B_5^-$ at (a) 355 nm, (b) 266 nm, and (c) 193 nm.

band D (VDE: ~4.42 eV), which may also contain multiple transitions.

D. $Ta_2B_5^-$

The 355 nm spectrum of $Ta_2B_5^-$ (Fig. 4(a)) exhibits five detachment transitions and a low energy tail labeled as "*." Band X with a VDE of 1.93 eV is relatively broad, suggesting a significant geometry change between the ground states of $Ta_2B_5^-$ and Ta_2B_5. The ADE of band X is estimated to be 1.83 ± 0.04 eV, which represents the EA of Ta_2B_5. The band A with a VDE of 2.23 eV is relatively sharp. Band B with a VDE of 2.70 eV is not well resolved at 355 nm, but better defined in the 266 and 193 nm spectra. VDEs of bands C and D are measured to be 2.87 and 3.10 eV, respectively. At 266 nm (Fig. 4(b)), a band E with a VDE of 3.54 eV is well resolved. However, Both the 266 and 193 nm spectra show that the higher binding energy side is very congested. Two bands, F (VDE: 4.01 eV) and G (VDE ~4.7 eV), are labeled for the sake of discussion. The low energy tail "*" is likely due to contributions of a low-lying isomer.

V. THEORETICAL RESULTS

The optimized anion ($Ta_2B_x^-$) and neutral (Ta_2B_x) ground states and low-lying isomers (within ~0.50 eV) at the BP86 level are presented in Figs. 5–8 for x = 2–5,

TABLE I. Experimental vertical detachment energies (VDEs) from the photoelectron spectra of $Ta_2B_x^-$ ($x = 2-5$), compared to the calculated VDEs at the BP86 level from the anion ground state.[a]

Observed feature	VDE (Expt.)[b]	VDE (Theor.)[c]	MO
$Ta_2B_2^-$			
X	1.39 (4)	1.45(S)	$9a_1$ (α)
A	2.28(5)	1.95(T)	$2a_2$ (β)
		2.02(S)	$2a_2$ (α)
		2.17(T)	$8a_1(\beta)$
		2.18(T)	$4b_1(\beta)$
		2.27(S)	$4b_1$ (α)
B	2.78(5)	2.34(S)	$8a_1(\alpha)$
		3.19(T)	$4b_2(\beta)$
		3.20(T)	$7a_1(\beta)$
C	3.35(3)	3.33(S)	$4b_2$ (α)
		3.37(S)	$7a_1(\alpha)$
D	3.66(4)	3.67(T)	$6a_1(\beta)$
E	3.98(4)	3.77(S)	$6a_1(\alpha)$
$Ta_2B_3^-$			
X	2.00(3)	2.00(Q)	$5b_1(\beta)$
A	2.16(3)	2.23(D)	$5b_2(\alpha)$
		2.27(Q)	$2a_2(\beta)$
		2.28(D)	$10a_1(\alpha)$
		2.36(D)	$5b_1(\alpha)$
B	2.75(3)	2.72(Q)	$9a_1(\beta)$
		2.74(D)	$2a_2(\alpha)$
C	3.17(3)	3.33(D)	$9a_1(\alpha)$
		3.35(Q)	$4b_1(\beta)$
D	3.96(6)	3.79(D)	$4b_1(\alpha)$
		4.07(Q)	$8a_1(\beta)$
		4.16(Q)	$4b_2(\beta)$
E	4.69(6)	4.57(D)	$8a_1(\alpha)$
$Ta_2B_4^-$			
X	~1.9	2.05(S)	$11a_1$ (α)
		2.12(T)	$5b_1(\beta)$
		2.23(S)	$5b_1(\alpha)$
A	2.43 (4)	2.37(T)	$10a_1(\beta)$
		2.39(S)	$10a_1(\alpha)$
B	2.88(6)	2.65(S)	$2a_2(\alpha)$
		2.67(T)	$2a_2(\beta)$
		2.94(S)	$6b_2(\alpha)$
		3.00(T)	$6b_2(\beta)$
C	3.81(3)	3.89(T)	$9a_1(\beta)$
		4.04(S)	$9a_1(\alpha)$
D	4.42(6)	4.29(T)	$5b_2(\beta)$
		4.30(S)	$5b_2(\alpha)$
		4.54(T)	$8a_1(\beta)$
		4.54(S)	$8a_1(\alpha)$
$Ta_2B_5^-$			
X	1.93(4)	2.02(D)	$3a_2(\alpha)$
A	2.23(3)	2.38(D)	$11a_1(\alpha)$
B	2.70(4)	2.71(D)	$5b_1(\alpha)$
C	2.87(4)	2.74(D)	$7b_2(\alpha)$
D	3.10(4)	2.93(D)	$6b_2(\alpha)$
E	3.54(4)	3.30(D)	$10a_1(\alpha)$
F	4.01(8)	4.44(D)	$9a_1(\alpha)$
G	4.7(1)	4.87(D)	$4b_1(\alpha)$

[a]All energy are in eV.
[b]Numbers in parentheses represent the uncertainty in the last digit.
[c]VDEs were calculated at BP86 level: S, singlet final states; D, doublet final states; T, triplet final states; Q, quartet final states.

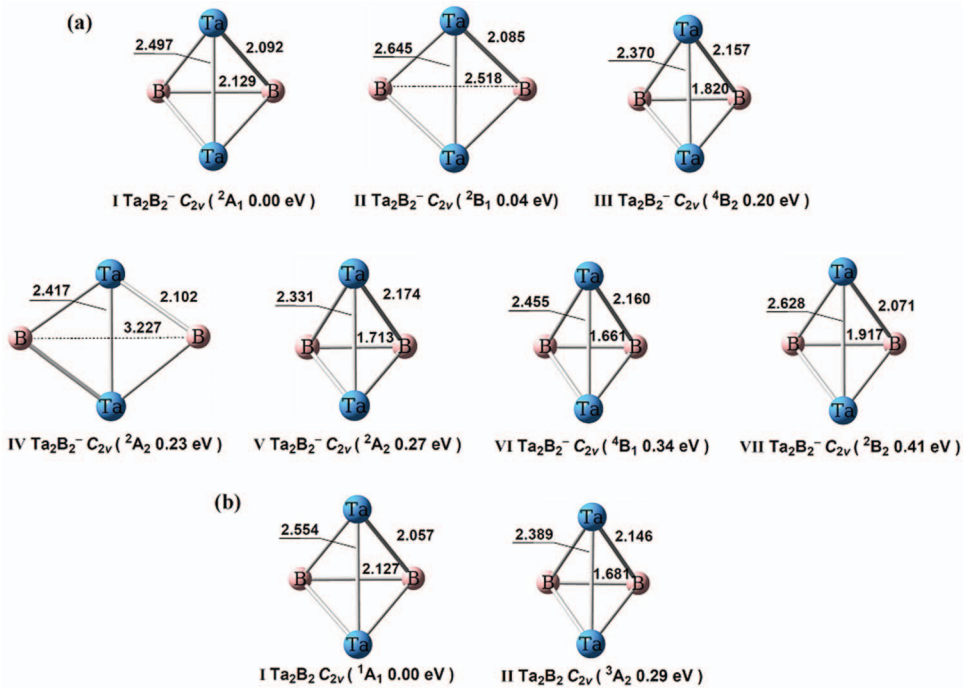

FIG. 5. (a) Optimized low-lying structures for $Ta_2B_2^-$ at the BP86 level of theory. (b) Optimized low-lying structures for Ta_2B_2 at the BP86 level of theory. The bond lengths are in Å.

respectively. More optimized geometries at higher energies are given as supplementary material (Figs. S1–S8).[52]

A. $Ta_2B_2^-$ and Ta_2B_2

The structures for $Ta_2B_2^-$ and Ta_2B_2 are extensively searched and optimized at the BP86 level with different spin states. The optimized ground states and selected low-lying isomers within 0.50 eV for $Ta_2B_2^-$ and Ta_2B_2 are presented in Fig. 5. The ground state of $Ta_2B_2^-$ has a C_{2v} ($^2A_1$) geometry (Fig. 5(a)-I), in which the Ta–Ta bond is perpendicular to the B–B bond in a distorted tetrahedral shape. Isomer (Fig. 5(a)-II) (C_{2v}, $^2B_1$) with a much longer B–B bond is only 0.04 eV higher in energy, essentially degenerate with the ground state within the accuracy of our calculations. To resolve the true ground state of $Ta_2B_2^-$, we performed optimizations for these two isomers in CCSD(T) calculations with the Ta/Stuttgart + 2*f*1*g*/B/aug-cc-pVTZ basis sets. The results show that the isomer (Fig. 5(a)-I) is the ground state, but isomer (Fig. 5(a)-II) is still very close only 0.05 eV higher using the CCSD(T) optimized structures (Table SI).[52] Thus, isomer (Fig. 5(a)-II) may also contribute to the experimental observation. Other selected low-lying isomers are at least 0.20 eV higher in energy, which are not competitive for the global minimum.

The global minimum of Ta_2B_2 ($^1A_1$, C_{2v}) (Fig. 5(b)-I) has a slightly longer Ta–Ta bond (0.05 Å) compared to that of the anion (Fig. 5(a)-I). The second low-lying isomer is 0.29 eV higher in energy with a remarkably shorter B–B bond (1.681 Å) as shown in Fig. 5(b)-II.

B. $Ta_2B_3^-$ and Ta_2B_3

The ground state of $Ta_2B_3^-$ is open-shell with a triplet electronic state ($^3B_2$) and C_{2v} symmetry (Fig. 6(a)-I). It can be viewed as a quasi-bipyramidal structure with the Ta–Ta dimer interacting perpendicularly with a bent B_3 chain. The corresponding closed-shell state (Fig. 6(a)-IV) is 0.17 eV higher in energy. A low symmetry C_s ($^1A'$) structure (Fig. 6(a)-II) with a shorter Ta–Ta bond is 0.12 eV above the ground state and its corresponding triplet state is 0.34 eV above the ground state (Fig. 6(a)-VI). A very low symmetry C_1 (^1A) structure (Fig. 6(a)-III) is 0.17 eV above the ground state, featuring a boron atom interacting with only one other B and Ta atom on a quasi-tetrahedral Ta_2B_2 core.

For the neutral Ta_2B_3 cluster, six low-lying isomers are found within 0.10 eV at the BP86 level. The ground state is a C_{2v} ($^4A_2$) structure (Fig. 6(b)-I), similar to the global minimum of $Ta_2B_3^-$. Further theoretical calculations at the CCSD(T) level are performed for these low-lying isomers to resolve the true ground state, as reported in Table SI.[52] The CCSD(T) results show that the C_2 (^2B) structure (Fig. 6(b)-VI), which is also similar to the anion ground state, but 0.08 eV above the C_{2v} ($^4A_2$) structure at the BP86 level, is the global minimum, whereas the C_{2v} ($^4A_2$) structure is 0.17 eV higher than the C_2 (^2B) state at the higher level of calculation.

C. $Ta_2B_4^-$ and Ta_2B_4

The ground state of $Ta_2B_4^-$ ($^2A_1$, C_{2v}) (Fig. 7(a)-I) can be viewed as extending the B_3 chain in the $Ta_2B_3^-$ global minimum structure to form a bent B_4 chain. Interestingly, while the Ta–Ta distance is similar in the two clusters, the B–B bond lengths seem to be shortened significantly in $Ta_2B_4^-$ relative to those in $Ta_2B_3^-$. There are only two other isomers within 0.50 eV of the ground state and they are at least 0.4 eV higher in energy (Figs. 7(a)-II and 7(a)-III).

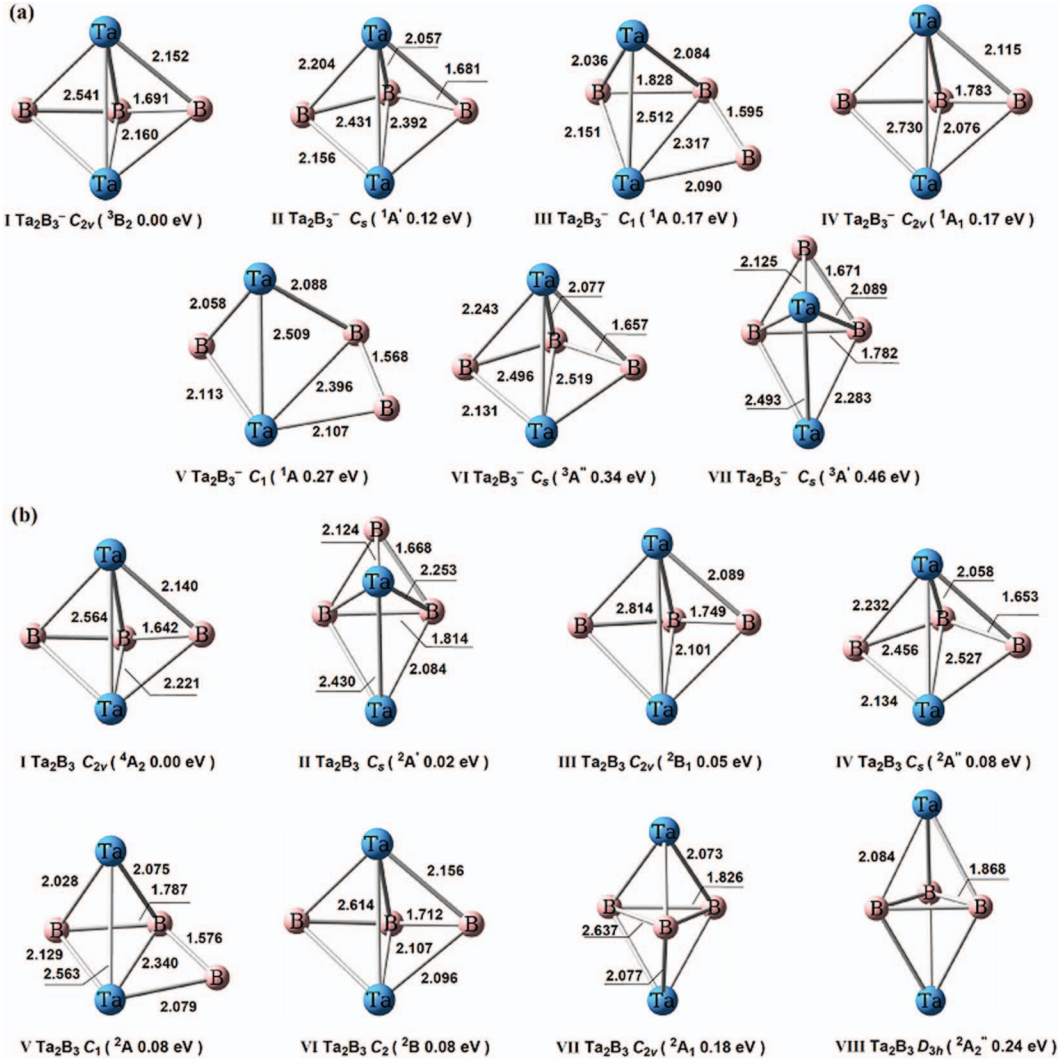

FIG. 6. (a) Optimized low-lying structures for $Ta_2B_3^-$ at the BP86 level of theory. (b) Optimized low-lying structures for Ta_2B_3 at the BP86 level of theory. The bond lengths are in Å.

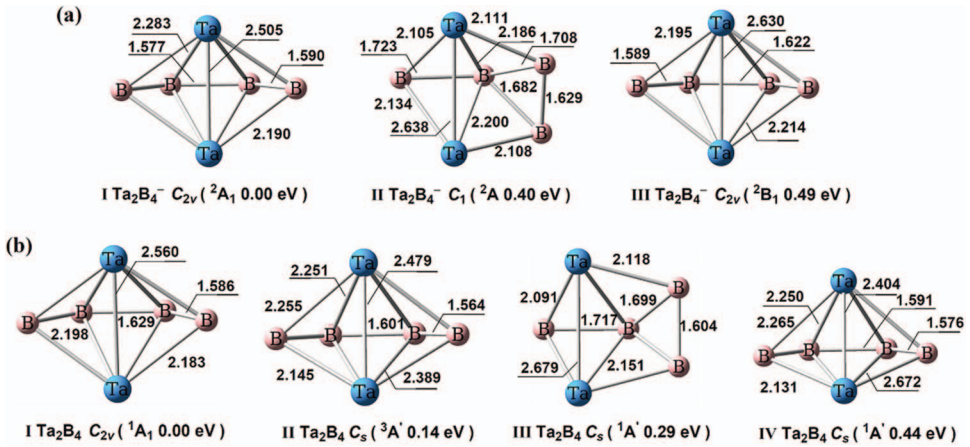

FIG. 7. (a) Optimized low-lying structures for $Ta_2B_4^-$ at the BP86 level of theory. (b) Optimized low-lying structures for Ta_2B_4 at the BP86 level of theory. The bond lengths are in Å.

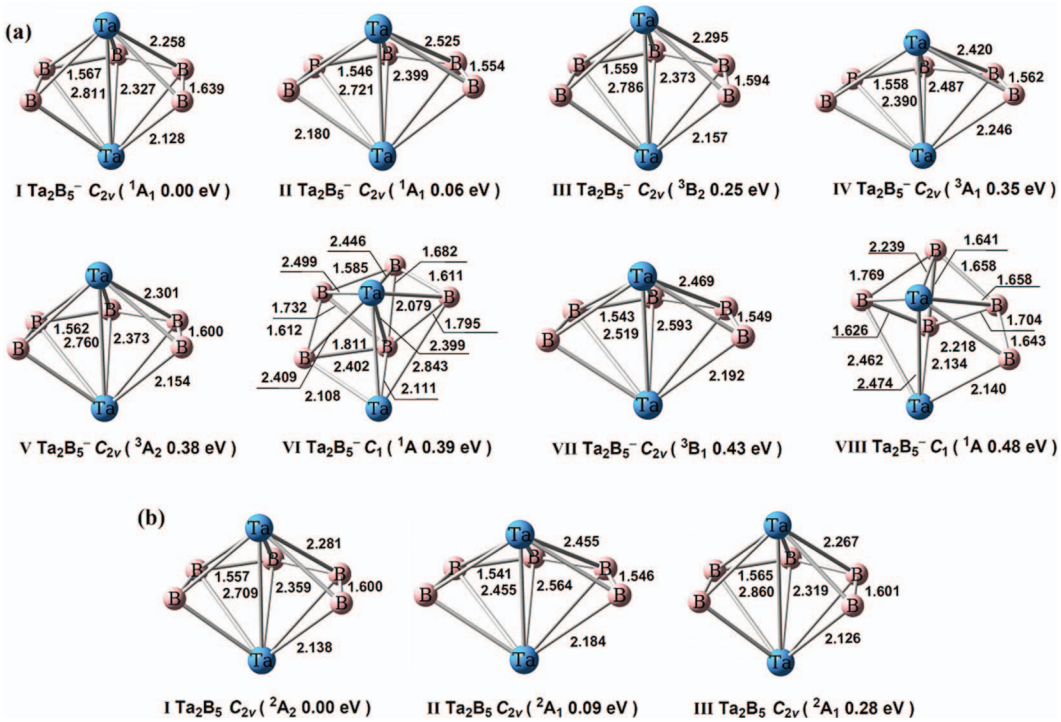

FIG. 8. (a) Optimized low-lying structures for $Ta_2B_5^-$ at the BP86 level of theory. (b) Optimized low-lying structures for Ta_2B_5 at the BP86 level of theory. The bond lengths are in Å.

The low-lying isomers of the neutral Ta_2B_4 are depicted in Fig. 7(b). The global minimum (Fig. 7(b)-I) resembles that of $Ta_2B_4^-$, except a slightly lengthened Ta–Ta bond (by 0.06 Å) and the middle B–B bond (by 0.05 Å). The low-lying isomer (Fig. 7(b)-II) with C_s symmetry is a triplet state ($^3A'$), only 0.14 eV above the ground state. The other two low-lying isomers are also of C_s symmetry and are closed-shell (Figs. 7(b)-III and 7(b)-IV).

D. $Ta_2B_5^-$ and Ta_2B_5

The low-lying isomers for $Ta_2B_5^-$ are given in Fig. 8(a). Eight structures are found to be within 0.50 eV at BP86 level. The ground state (Fig. 8(a)-I) has a five-member bent boron chain with C_{2v} ($^1A_1$) symmetry. A very competitive isomer (Fig. 8(a)-II) with a shorter Ta–Ta bond is only 0.06 eV higher in energy. Single-point CCSD(T) calculations are performed using the BP86 geometries, showing isomer (Fig. 8(a)-II) is 0.21 eV higher than isomer (Fig. 8(a)-I) at the higher level of theory (Table SI).[52] The third isomer (Fig. 8(a)-III) is a triplet state ($^3B_2$) also with C_{2v} symmetry and is 0.25 eV above the singlet ground state. The other structures in Fig. 8(a) are at least 0.35 eV above the global minimum.

For the neutral Ta_2B_5, two competitive low-lying isomers are found at the BP86 level, which are similar to the two low-lying isomers of the anion. Single-point CCSD(T) calculations are performed for the neutral Ta_2B_5 low-lying isomers, revealing that isomer 8b-II is 0.23 eV higher than 8b-I (Table SI).[52] The third low-lying isomer C_{2v} ($^2A_1$) (Fig. 8(b)-III) is 0.28 eV higher in energy at the BP86 level.

VI. COMPARISON BETWEEN EXPERIMENT AND THEORY

In order to verify the global minimum and low-lying structures of $Ta_2B_x^-$ ($x = 2-5$), we have calculated the VDEs on the basis of the identified anionic structures with the generalized Koopmans' theorem. The calculated VDEs and simulated PES spectra for the ground state structures are compared with the experiment data in Table I and Fig. 9. The simulated PES spectra for all the low-lying structures of the anions are compared with the experimental spectra in Figs. S9−S12 in the supplementary material for $Ta_2B_x^-$ ($x = 2-5$), respectively.[52] In the single-particle picture, photodetachment involves removal of electrons from occupied MOs of an anion. The final states are the ground and excited states of the corresponding neutral. Considering the complicated nature of the electronic structures of these systems, we can only make qualitative comparisons between experiment and theory in some cases.

A. $Ta_2B_2^-$

The ground state of $Ta_2B_2^-$ (Fig. 5(a)-I) is open-shell with a valence configuration of $\ldots(5a_1)^2(3b_1)^2(6a_1)^2(7a_1)^2(4b_2)^2(8a_1)^2(4b_1)^2(2a_2)^2(9a_1)^1$. As shown in Fig. 9(a), the simulated PES spectrum from the global minimum of $Ta_2B_2^-$ agrees well with the experimental spectrum. The $9a_1$ SOMO of $Ta_2B_2^-$ (Fig. 10(a)) is primarily a Ta–Ta nonbonding σ orbital. The Mülliken spin density (Fig. 10(c)) shows that the unpaired spin is equally shared by the two Ta atoms. On removal of an electron, the HOMO ($4b_1$) of the neutral (Fig. 10(b)) is shown to be a δ bonding orbital and the neutral

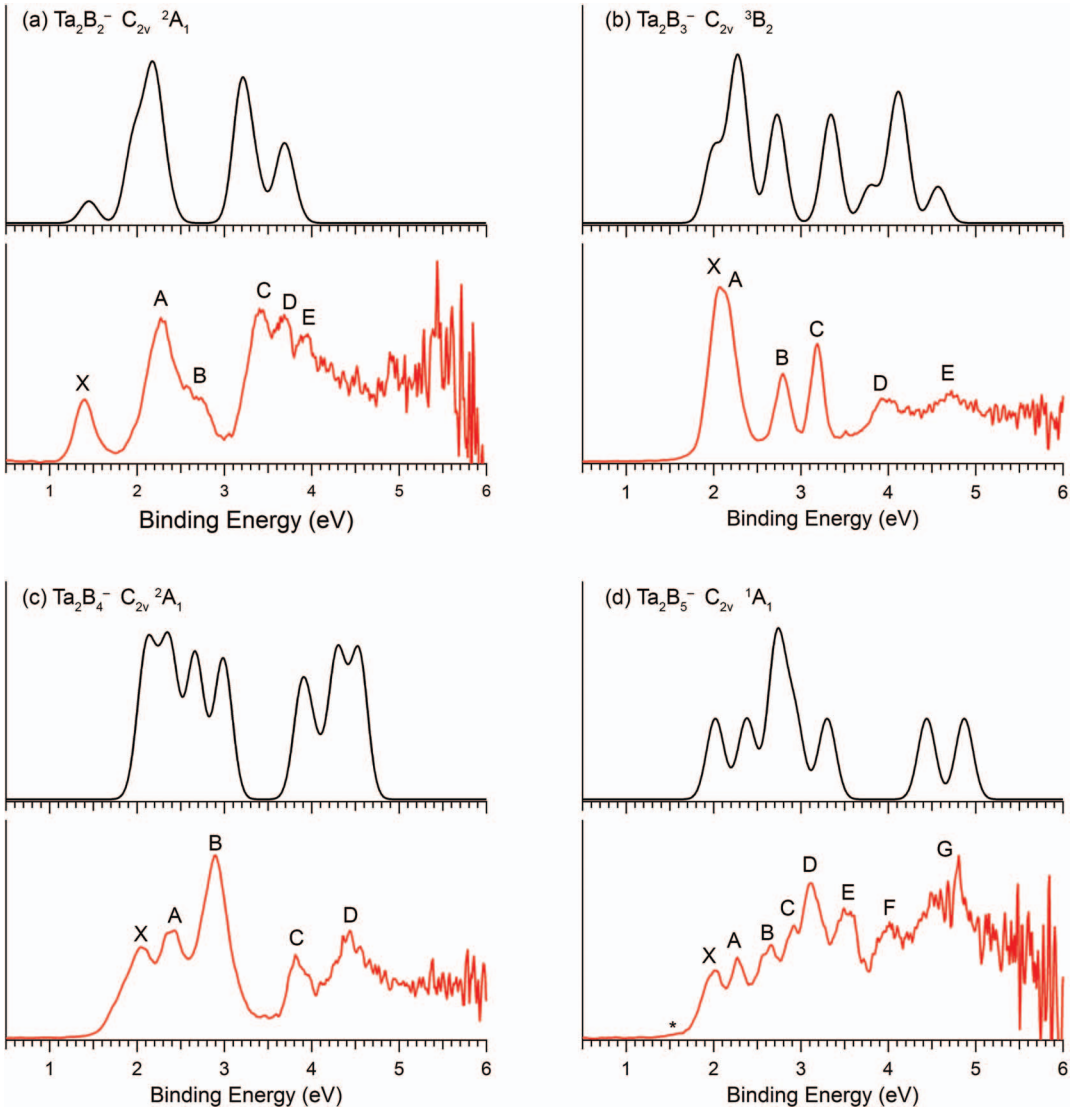

FIG. 9. Comparison of the 193 nm photoelectron spectra of $Ta_2B_x^-$ ($x = 2-5$) with the simulated spectra from the lowest energy structures. The simulated spectra were made by fitting the calculated VDEs with unit-area Gaussian functions of 0.10 eV width.

Ta_2B_2 remains the C_{2v} structure with a shorter Ta–Ta bond by about 0.06 Å. The first calculated VDE (1.45 eV), corresponding to the electron detachment from the $9a_1$ SOMO is in good agreement with the experimental VDE of band X (1.39 eV, Table I). Detachment from the fully occupied MOs below the $9a_1$ SOMO can lead to both singlet (S) and triplet (T) final states. At the BP86 level, the calculated VDEs from the $2a_2$ (T, S), $8a_1$ (T), and $4b_1$ (T, S) orbitals are very close to each other ranging from 1.95 to 2.27 eV, consistent with the intense and broad A band. The calculated VDEs for the higher binding energy features are also in qualitative agreement with the observed spectral pattern, as shown in Table I and Fig. 9(a).

The simulated spectrum of isomer (Fig. 5(a)-II) (C_{2v}, $^2B_1$) is shown in Fig. S9.[52] The overall pattern also shows good agreement with the experimental spectrum, except that the first calculated VDE for isomer (Fig. 5(a)-II) is higher than that for the ground state isomer (Fig. 5(a)-I). Thus, the first detachment band from isomer (Fig. 5(a)-II) should appear as a shoulder to the higher binding energy side of the X band (Fig. 1). The lack of a clear shoulder in the experimental spectra suggests that contributions from isomer (Fig. 5(a)-II) are negligible, even though it cannot be completely ruled out. Thus, the overall agreement between the simulated spectrum for the ground state structure and the experimental results lends credence to the C_{2v} ($^2A_1$) structure (Fig. 5(a)-I) as the global minimum for $Ta_2B_2^-$.

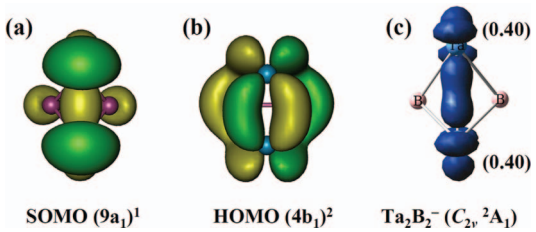

FIG. 10. (a) The SOMO picture of $Ta_2B_2^-$ (C_{2v}, $^2A_1$). (b) The HOMO picture of Ta_2B_2 (C_{2v}, $^1A_1$). (c) The Mülliken spin density of $Ta_2B_2^-$ (C_{2v}, $^2A_1$).

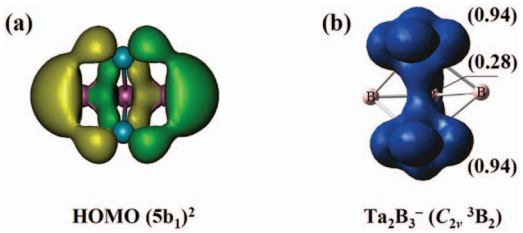

FIG. 11. (a) The HOMO picture of $Ta_2B_3^-$ (C_{2v}, $^3B_2$). (b) The Mülliken spin density of $Ta_2B_3^-$ (C_{2v}, $^3B_2$).

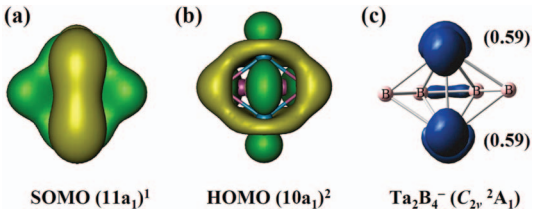

FIG. 12. (a) The SOMO picture of $Ta_2B_4^-$ (C_{2v}, $^2A_1$). (b) The HOMO picture of Ta_2B_4 (C_{2v}, $^1A_1$). (c) The Mülliken spin density of $Ta_2B_4^-$ (C_{2v}, $^2A_1$).

B. $Ta_2B_3^-$

The simulated spectrum for the global minimum of $Ta_2B_3^-$ is found to agree well with the experimental spectrum (Fig. 9(b)). The ground state of $Ta_2B_3^-$ (Fig. 6(a)-I) is a triplet state with a valence configuration of $\ldots(6a_1)^2(3b_1)^2(7a_1)^2(4b_2)^2(8a_1)^2(4b_1)^2(9a_1)^2(2a_2)^2(5b_1)^2(10a_1)^1(5b_2)^1$. The first detachment channel corresponds to electron removal from the HOMO ($5b_1$), which is basically a δ-bonding orbital (Fig. 11(a)). The calculated VDE of 2.00 eV at the BP86 level is in excellent agreement with the experimental observation at 2.00 eV. There are four close-lying detachment channels with calculated VDEs ranging from 2.23 to 2.36 eV (Table I), which are tentatively assigned to the A band. This assignment is tentative because the A band is relatively sharp and is inconsistent with so many detachment channels. However, the calculated VDEs for the higher binding energy channels seem to be in good agreement with the experiment, as can be seen from Table I and Fig. 9(b).

The second isomer of $Ta_2B_3^-$ (Fig. 6(a)-II) is closed shell with C_s symmetry ($^1A'$), which is 0.12 eV higher in energy at BP86 level. The simulated spectrum of this isomer (Fig. S10)[52] also seems to be consistent with the experimental spectrum. Thus, at the current level of theory, we cannot assign definitively which isomer is responsible for the observed spectra. Both structures are similar, except that the C_s isomer features a slightly stronger and shorter Ta–Ta bond.

C. $Ta_2B_4^-$

The C_{2v} ($^2A_1$) structure (Fig. 7(a)-I) is clearly the ground state for $Ta_2B_4^-$ with alternative structures being at least 0.40 eV higher in energy. The valence electron configuration of the $Ta_2B_4^-$ ground state is $\ldots(7a_1)^2(4b_1)^2(8a_1)^2(5b_2)^2(9a_1)^2(6b_2)^2(2a_2)^2(10a_1)^2(5b_1)^2(11a_1)^1$. The X band in the experimental spectra is broad and congested, suggesting that it may contain multiple detachment channels. Indeed, the calculated VDEs for the first three detachment channels, from the SOMO $11a_1$ and the $5b_1$ orbital (T and S), are very close to each other (Table I), consistent with the broad X band. The $11a_1$ SOMO is mainly a Ta–Ta σ bonding orbital, as shown in Fig. 12(a) and Fig. 12(c) for the spin density. Detachment of the electron in the SOMO leads to a slightly increased Ta–Ta bond length in the neutral ground state of Ta_2B_4 (Fig. 7(b)-I). The calculated VDEs from the $10a_1$ orbital, 2.37 eV (T) and 2.39 eV (S), corresponding to the removal of the spin-down and spin-up electrons, are in good agreement the observed VDE of the A band (2.43 eV). The $10a_1$ orbital, which is primarily a $\sigma_{d\text{-}d}$ bonding orbital (Fig. 12(b)), becomes the HOMO of the closed-shell neutral Ta_2B_4 cluster. Each of the subsequent experimental spectral features also corresponds to multiple detachment channels. Overall, the calculated spectral pattern from the global minimum of $Ta_2B_4^-$ is in good agreement with the experimental observation (Table I and Fig. 9(c)), lending considerable credence to the global minimum identified.

D. $Ta_2B_5^-$

The comparisons between experiment and theory for the ground state of $Ta_2B_5^-$ are presented in Table I and Fig. 9(d). The ground state of $Ta_2B_5^-$ is closed shell ($^1A_1$) with a configuration of $\ldots(4b_2)^2(8a_1)^2(5b_2)^2(4b_1)^2(9a_1)^2(10a_1)^2(6b_2)^2(2a_2)^2(7b_2)^2(5b_1)^2(11a_1)^2(3a_2)^2$. The first calculated VDE corresponds to electron detachment from the $3a_2$ HOMO, which is an antibonding δ orbital (Fig. 13(a)). The SOMO ($3a_2$) of the neutral cluster upon removing an electron from the anion HOMO is shown in Fig. 13(b) and its spin density (Fig. 13(c)) is seen to concentrate on the two Ta atoms. The calculated VDE of 2.02 eV is in good agreement with the experimental value of 1.93 eV (Table I). The next two calculated VDEs correspond to electron detachments from HOMO-1 ($11a_1$) and HOMO-2 ($5b_1$), which are in good agreement with the experimental bands A and B, respectively. The next three detachment channels are derived from the $7b_2$, $2a_2$, and $6b_2$, which correspond to the bands C, D, and E at VDEs of 2.87, 3.10, and 3.54 eV in the experimental spectra, respectively. The higher detachment channels are also in good agreement with the experiment.

The weak feature on the low binding energy side of the experimental spectra of $Ta_2B_5^-$ (Fig. 4) suggests possible contributions from low-lying isomers. The second low-lying isomer Fig. 8(a)-II is 0.06 eV and 0.23 eV higher in energy at BP86 and CCSD(T) level of theory (Table SI),[52] respectively.

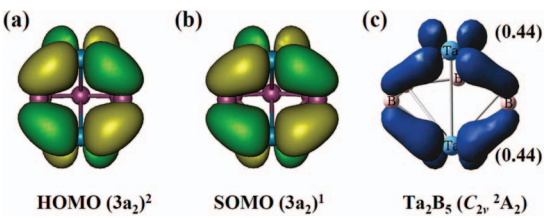

FIG. 13. (a) The HOMO picture of $Ta_2B_5^-$ (C_{2v}, $^1A_1$). (b) The SOMO picture of Ta_2B_5 (C_{2v}, $^2A_2$). (c) The Mülliken spin density of Ta_2B_5 (C_{2v}, $^2A_2$).

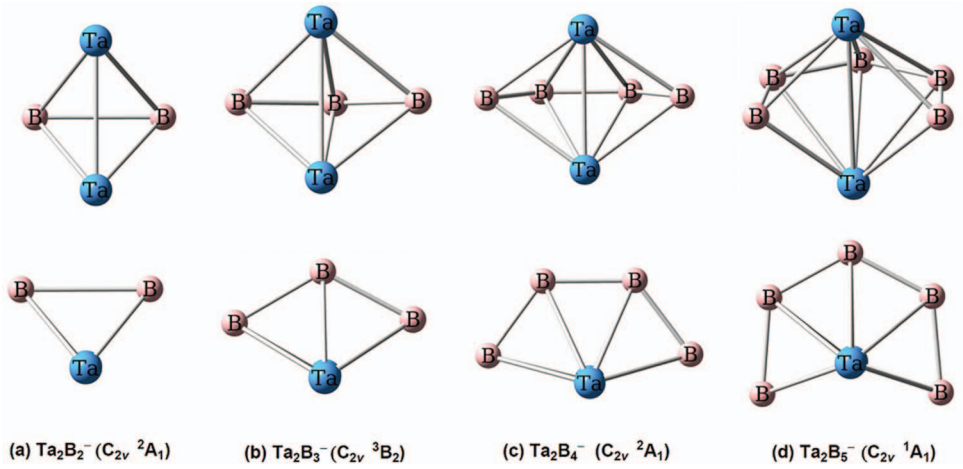

FIG. 14. Structure evolution of $Ta_2B_x^-$ ($x = 2-5$). Geometries in the second row are projections viewing along the Ta–Ta axis.

The simulated spectrum for this isomer (Fig. S12)[52] shows that its binding energies are similar to those of the global minimum. Thus, this isomer can be ruled out to be the contributor to the low binding energy feature, in agreement with its relatively high energy at the CCSD(T) level. The third isomer (Fig. 8(a)-III) is open-shell ($^3B_2$), which is 0.25 eV above the global minimum at BP86. However, the VDE of its detachment channel (Fig. S12)[52] is at a lower binding energy and this isomer is a possible contributor to the observed low binding energy feature. Thus, at higher level of theory, we expect that the relatively energy of this isomer should be lower than the BP86 calculation suggests. Therefore, overall the theoretical results are in good agreement with the experimental data, confirming the ground state and low-lying isomers for the $Ta_2B_5^-$ cluster.

VII. STRUCTURAL EVOLUTION

The current study shows that the structures of the $Ta_2B_x^-$ ($x = 2-5$) clusters are all related and can be viewed as forming an equatorial boron belt around a Ta–Ta dimer with increasing x, as shown in Fig. 14. Starting from the C_{2v} $Ta_2B_2^-$, each additional B atom is added to the boron moiety to extend the boron chain around the Ta–Ta bond (Fig. 14). Even though in a couple of cases the global minimum structures cannot be definitively assigned, this basic structural evolution holds true because all the low-lying isomers of $Ta_2B_x^-$ display similar structures with the same B-B connectivity. The structural evolution is due to the strong B–B bonding, which leads to the formation of monotantalum metal-centered B_{10} ring in $Ta©B_{10}^-$.[20] Thus, we expect that with additional B atoms one may also achieve a closed equatorial boron ring around the Ta–Ta bond. In fact, we already see that the Ta–Ta bond length in $Ta_2B_5^-$ (Fig. 8(a)-I) is significantly longer than that in $Ta_2B_4^-$ (Fig. 7(a)-I), en route to a closed boron ring with a bipyramidal structure with a much longer Ta–Ta distance. Further studies of larger dinuclear boron clusters to observe such structures would be interesting and are forthcoming.

VIII. CONCLUSIONS

We present a systematic study of the $Ta_2B_x^{-/0}$ ($x = 2-5$) clusters using photoelectron spectroscopy and DFT calculations. Photoelectron spectra were obtained for the size-selected anionic clusters, revealing congested electronic transitions for all systems. Extensive DFT calculations were performed at the BP86 level to locate the ground states and low-lying isomers for the $Ta_2B_x^{-/0}$ ($x = 2-5$) clusters. Qualitative agreement between the experimental data and theoretical calculations was obtained, lending support for the global minimum structures from the DFT calculations. The ground states of $Ta_2B_x^-$ ($x = 2-5$) are shown to possess C_{2v} ($^2A_1$), C_{2v} ($^3B_2$), C_{2v} ($^2A_1$), and C_{2v} ($^1A_1$) structures, respectively, which can all be viewed as a partial equatorial boron ring around a Ta–Ta bond. The global minima of the neutral clusters follow the same pattern and are similar to the respective anions. The current results reveal that the strong boron–boron bonding dominates the structures of the di-tantalum clusters.

ACKNOWLEDGMENTS

This study was supported by the Natural Science Foundation of China (Grant Nos. 21071031 and 90922022 to X.H.) for the computational work and the U.S. National Science Foundation (Grant No. DMR-0904034 to L.-S.W.) for the experimental work.

[1]H. Hubert, B. Devouard, L. A. J. Garvie, M. O'Keeffe, P. R. Buseck, W. T. Petuskey, and P. F. McMillan, Nature (London) **391**, 376 (1998).
[2]M. Fujimori, T. Nakata, T. Nakayama, E. Nishibori, K. Kimura, M. Takata, and M. Sakata, Phys. Rev. Lett. **82**, 4452 (1999).
[3]H. Y. Chung, M. B. Weinberger, J. B. Levin, R. W. Cumberland, A. Kaver, J. M. Yang, S. H. Tolbert, and R. B. Kaner, Science **316**, 436 (2007).
[4]A. R. Oganov, J. H. Chen, C. Gatti, Y. Z. Ma, Y. M. Ma, C. W. Glass, Z. X. Liu, T. Yu, O. O. Kurakevych, and V. L. Solozhenko, Nature (London) **457**, 863 (2009).
[5]H. J. Zhai, A. N. Alexandrova, K. A. Birch, A. I. Boldyrev, and L. S. Wang, Angew. Chem. Int. Ed. **42**, 6004 (2003).
[6]H. J. Zhai, B. Kiran, J. Li, and L. S. Wang, Nat. Mater. **2**, 827 (2003).
[7]A. P. Sergeeva, D. Y. Zubarev, H. J. Zhai, A. I. Boldyrev, and L. S. Wang, J. Am. Chem. Soc. **130**, 7244 (2008).

[8]W. Huang, A. P. Sergeeva, H. J. Zhai, B. B. Averkiev, L. S. Wang, and A. I. Boldyrev, Nat. Chem. **2**, 202 (2010).
[9]B. Kiran, S. Bulusu, H. J. Zhai, S. Yoo, X. C. Zeng, and L. S. Wang, Proc. Natl. Acad. Sci. U.S.A. **102**, 961 (2005).
[10]Z. A. Piazza, W. L. Li, C. Romanescu, A. P. Sergeeva, L. S. Wang, and A. I. Boldyrev, J. Chem. Phys. **136**, 104310 (2012).
[11]A. P. Sergeeva, Z. A. Piazza, C. Romanescu, W. L. Li, A. I. Boldyrev, and L. S. Wang, J. Am. Chem. Soc. **134**, 18065 (2012).
[12]E. Oger, N. R. M. Crawford, R. Kelting, P. Weis, M. M. Kappes, and R. Ahlrichs, Angew. Chem. Int. Ed. **46**, 8503 (2007).
[13]B. B. Averkiev, D. Y. Zubarev, L. M. Wang, W. Huang, L. S. Wang, and A. I. Boldyrev, J. Am. Chem. Soc. **130**, 9248 (2008).
[14]L. M. Wang, W. Huang, B. B. Averkiev, A. I. Boldyrev, and L. S. Wang, Angew. Chem. Int. Ed. **46**, 4550 (2007).
[15]W. L. Li, C. Romanescu, T. R. Galeev, L. S. Wang, and A. I. Boldyrev, J. Phys. Chem. A **115**, 10391 (2011).
[16]C. Romanescu, A. P. Sergeeva, W. L. Li, A. I. Boldyrev, and L. S. Wang, J. Am. Chem. Soc. **133**, 8646 (2011).
[17]T. R. Galeev, C. Romanescu, W. L. Li, L. S. Wang, and A. I. Boldyrev, J. Chem. Phys. **135**, 104301 (2011).
[18]C. Romanescu, T. R. Galeev, W. L. Li, A. I. Boldyrev, and L. S. Wang, Angew. Chem. Int. Ed. **50**, 9334 (2011).
[19]W. L. Li, C. Romanescu, T. R. Galeev, Z. A. Piazza, A. I. Boldyrev, and L. S. Wang, J. Am. Chem. Soc. **134**, 165 (2012).
[20]T. R. Galeev, C. Romanescu, W. L. Li, L. S. Wang, and A. I. Boldyrev, Angew. Chem. Int. Ed. **51**, 2101 (2012).
[21]Q. Luo, Sci. China Ser. B: Chem. **51**, 607 (2008).
[22]K. Ito, Z. Pu, Q. S. Li, and P. V. R. Schleyer, Inorg. Chem. **47**, 10906 (2008).
[23]S. D. Li, C. Q. Miao, and J. C. Guo, Sci. China Ser. B: Chem. **52**, 900 (2009).
[24]Q. Y. Wu, Y. P. Tang, and X. H. Zhang, Sci. China Ser. B: Chem. **52**, 288 (2009).
[25]Z. F. Pu, K. Ito, P. V. Schleyer, and Q. S. Li, Inorg. Chem. **48**, 10679 (2009).
[26]W. L. Li, C. Romanescu, Z. A. Piazza, and L. S. Wang, Phys. Chem. Chem. Phys. **14**, 13663 (2012).
[27]B. P. T. Fokwa and M. Hermus, Angew. Chem., Int. Ed. **51**, 1702 (2012).
[28]K. A. Nguyen and K. Lammertsma, J. Phys. Chem. A **102**, 1608 (1998).
[29]H. J. Zhai, L. S. Wang, D. Y. Zubarev, and A. I. Boldyrev, J. Phys. Chem. A **110**, 1689 (2006).
[30]A. N. Alexandrova, E. Koyle, and A. I. Boldyrev, J. Mol. Model. **12**, 569 (2006).
[31]W. L. Li, C. Romanescu, T. Jian, and L. S. Wang, J. Am. Chem. Soc. **134**, 13228 (2012).
[32]L. S. Wang, H. S. Cheng, and J. Fan, J. Chem. Phys. **102**, 9480 (1995); L. S. Wang and X. Li, in *Advances in Metal and Semiconductor Clusters*, edited by M. A. Duncan (JAI, Greenwich, CT, 1998), Vol. 4, pp. 299–343.
[33]J. Akola, M. Manninen, H. Hakkinen, U. Landman, X. Li, and L. S. Wang, Phys. Rev. B **60**, R11297 (1999); L. S. Wang and X. Li, in *Proceedings of the International Symposium on Clusters and Nanostructure Interfaces, Richmond, VA, 25–28 October 1999*, edited by P. Jena, S. N. Khanna, and B. K. Rao (World Scientific, River Edge, NJ, 2000), pp. 293–300.
[34]H. Huang and L. S. Wang, Phys. Chem. Chem. Phys. **11**, 2663 (2009); W. Huang and L. S. Wang, Phys. Rev. Lett. **102**, 153401 (2009); H. Huang, S. Bulusu, R. Pal, X. C. Zeng, and L. S. Wang, ACS Nano **3**, 1225 (2009).
[35]A. D. Becke, Phys. Rev. A **38**, 3098 (1988).
[36]J. P. Perdew, Phys. Rev. B **33**, 8822 (1986).
[37]D. Andrae, U. Haeussermann, M. Dolg, H. Stoll, and H. Preuss, Theor. Chim. Acta **77**, 123 (1990).
[38]W. Küchle, M. Dolg, H. Stoll, and H. Preuss, Pseudopotentials of the Stuttgart/Dresden Group (revision: Tuesday, August 11, 1998), 1998. see http://www.theochem.uni-stuttgart.de/pseudopotentials.
[39]J. M. L. Martin and A. Sundermann, J. Chem. Phys. **114**, 3408 (2001).
[40]T. H. Dunning, J. Chem. Phys. **90**, 1007 (1989).
[41]R. A. Kendall, T. H. Dunning, and R. J. Harrison, J. Chem. Phys. **96**, 6796 (1992).
[42]G. D. Purvis III and R. J. Bartlett, J. Chem. Phys. **76**, 1910 (1982).
[43]G. E. Scuseria, C. L. Janssen, and H. F. Schaefer III, J. Chem. Phys. **89**, 7382 (1988).
[44]K. Raghavachari, G. W. Trucks, J. A. Pople, and M. Head-Gordon, Chem. Phys. Lett. **157**, 479 (1989).
[45]J. D. Watts, J. Gauss, and R. J. Bartlett, J. Chem. Phys. **98**, 8718 (1993).
[46]R. J. Bartlett and M. Musial, Rev. Mod. Phys. **79**, 291 (2007).
[47]M. J. Frisch, G. W. Trucks, H. B. Schlegel *et al.*, GAUSSIAN 03, Revision D.01, Gaussian, Inc., Wallingford, CT, 2004.
[48]H.-J. Werner, P. J. Knowles, F. R. Manby, M. Schütz *et al.*, MOLPRO, version 2010.1, a package of *ab initio* programs, 2010, see http://www.molpro.net.
[49]W. Humphrey, A. Dalke, and K. Schulten, J. Mol. Graphics **14**, 33 (1996).
[50]D. J. Tozer and N. C. Handy, J. Chem. Phys. **109**, 10180 (1998).
[51]L. S. Wang, J. Conceicao, C. Jin, and R. E. Smalley, Chem. Phys. Lett. **182**, 5 (1991); J. C. Pinare, B. Baguenard, C. Bordas, and M. Broyer, Phys. Rev. Lett. **81**, 2225 (1998).
[52]See supplementary material at http://dx.doi.org/10.1063/1.4776769 for the additional optimized structures, comparison of simulated spectra from low-lying isomers with experiment, CCSD(T) single point energies, and Cartesian coordinates for all optimized structures.